CHINESE OPTICS LETTERS

Vol. 21, No. 8 | August 2023

Temporal manipulation of spatiotemporal optical vortices with an Airy pulse [Invited]

Yimin Zang[1], Fanli Wei[1], Hee Sung Kim[2], and Andy Chong[2*]

[1] Department of Electro-Optics and Photonics, University of Dayton, Dayton, Ohio 45469, USA

[2] Department of Physics, Pusan National University, Busan 46241, Republic of Korea

*Corresponding author: chong0422@pusan.ac.kr

Received March 2, 2023 | Accepted April 23, 2023 | Posted Online August 8, 2023

We demonstrate the temporal manipulation of spatiotemporal optical vortices (STOVs) by utilizing Airy pulses. By combining a STOV with an Airy temporal profile, the STOV exhibits nondispersive, self-accelerating, and self-healing features inherited from the Airy pulse propagation. Such features will enhance the control of STOVs in time.

Keywords: spatiotemporal vortex; Airy pulse; manipulation.

DOI: 10.3788/COL202321.080002

1. Introduction

Optical vortex beams have been active research topics[1–3]. A variety of applications have been demonstrated, such as optical communications[4], optical spanners and tweezers[5], and optical imaging[6]. A typical vortex beam has a phase singularity in the transverse plane with orbital angular momentum (OAM) in the longitudinal direction[7]. Recently, a new type of vortex referred to as a spatiotemporal optical vortex (STOV) has been demonstrated[8,9]. The STOVs have phase singularities in the space–time domain with transverse OAM, which is a feature very distinct from traditional optical vortex beams.

In general, the STOV is not stable in propagation. In dispersive media propagation, the pulse broadening by the group velocity dispersion (GVD) will distort the wave packet severely to lose the phase singularity eventually[9]. A more robust STOV is desired to tolerate the propagation in a lengthy dispersive medium as an optical fiber. One idea is to combine STOVs with propagation-invariant localized waves[10] to preserve wave-packet structures against external perturbations, such as propagation in a dispersive medium. For example, a spatiotemporal Bessel structure has been explored to generate a nonspreading STOV[11]. Another profile one can use is the Airy pulse (beam), which exhibits not only dispersion (diffraction)-free propagation[12], but also other interesting propagation effects such as self-acceleration[13,14] and self-healing[15]. Due to their intriguing propagation characteristics, Airy beams have been utilized in applications such as curved plasma channel generation[16], particle clearing[17], optical imaging[18], and optical trapping[19-23]. Exploring unique propagation properties, combining Airy profiles with optical vortex beams has also been demonstrated in various previous research studies[24–27].

In this Letter, we combined an Airy pulse and a STOV to form an Airy–STOV wave packet to manipulate the STOV in time. Due to the Airy pulse's dispersion-free property, such an Airy–STOV wave packet maintains its temporal profile for long-distance propagation. Due to the self-healing property, it also self-heals against external perturbations. In addition, by the self-acceleration of the Airy–STOV wave packet, one can manipulate the phase singularity location in time as well.

2. Theory

An Airy pulse is generated by applying a third-order dispersion (TOD) in the frequency domain[28]. Meanwhile, a spiral phase is added in the spatial-frequency–frequency domain to form a STOV. We can combine the TOD and the spiral phase in the spatial-frequency–frequency domain to form an Airy–STOV wave packet, as shown in Eq. (1),

$$\tilde{E}(k_x, \omega; z) = g(r) e^{il\theta} e^{\frac{j\beta_3 z_0 \omega^3}{6}}. \tag{1}$$

The $g(r)$ is the radial Gaussian profile, l is the topological charge, β_3 is the TOD coefficient, and therefore $\beta_3 z_0$ is the total TOD, where $r = \sqrt{k_x^2 + \omega^2}$ and $\theta = \arctan(\omega/k_x)$. The two-dimensional (2D) inverse Fourier transform gives the spatiotemporal electric field of the Airy–STOV in the space–time domain,

$$E(x, t; z) = 2\pi(-i)^l G(\rho) e^{il\varnothing} \mathrm{Ai}(at)\delta(x), \quad \text{with } a = \left(\frac{2}{\beta_3 z_0}\right)^{\frac{1}{3}}. \tag{2}$$

The resulting spatiotemporal profile is shown in Eq. (2), where $\otimes$ represents the convolution, and $\rho = \sqrt{x^2 + t^2}$, $\varnothing = \arctan(t/x)$ and $G(\rho)$ is the Henkel transform of $g(r)$. As shown in Eq. (2), the resulting wave packet is the convolution of the STOV and the Airy pulse. Figure 1(a) shows the theoretical intensity profile of a typical Airy–STOV with topological charge $l = 1$. The convolution of the STOV results in multiple spatiotemporal phase singularities, as shown in the theoretical phase map [Fig. 1(b)]. The phase map indicates that all singularities have the same topological charge ($l = 1$ for this case).

The sign of β_3 determines the direction of the sidelobe tail. For $\beta_3 > 0$, the tail leads in time, as shown in Fig. 1. For $\beta_3 > 0$, the tail will lag in time. In case of a higher topological charge ($l \geq 2$), the STOV will split into multiple $l = 1$ STOVs as the Airy–STOV propagates[8,9].

To simulate the dispersion-free and the self-acceleration feature, a large amount of the GVD (quadratic phase of $\beta_2 z$ as a function of the propagation distance) is added to the Airy–STOV wave packet. In the spatial-frequency–frequency domain, the Airy–STOV propagation in a dispersive medium is shown in Eq. (3),

$$\tilde{E}(k_x, \omega; z) = g e^{il\varnothing} e^{i\beta_2 z\omega^2/2} e^{i\beta_3 z_0 \omega^3/6}. \tag{3}$$

After the 2D inverse Fourier transform, the spatiotemporal Airy–STOV propagation under the GVD effect is expressed in Eq. (4),

$$E(x, t; z) = 2\pi(-i)^l G(\rho) e^{il\varnothing} \otimes a \exp\left[-i\left(\frac{2\beta_2^3 z^3}{3\beta_3^2 z_0^2} + \frac{\beta_2 z}{\beta_3 z_0} t\right)\right] \times \mathrm{Ai}\left[a\left(t - \frac{\beta_2^2 z^2}{2\beta_3 z_0}\right)\right]\delta(x). \tag{4}$$

According to Eq. (4), the overall wave packet can be characterized as the STOV convoluted with the temporal shifted Airy pulse. The amount of the temporal shift is proportional to the propagation distance square, which is the feature of the free acceleration. If the GVD effect ($\beta_2 z$) is much smaller than the TOD ($\beta_3 z_0$), the GVD will not significantly change the Airy–STOV structure, which is referred to as the dispersion-free propagation. To observe an obvious dispersion-free phenomenon, a sufficiently large $\beta_3 z_0$ should be adopted. On the other hand, the temporal displacement is determined by $\frac{\beta_2^2 z^2}{2\beta_3 z_0}$, which indicates a larger amount of $\beta_3 z_0$ will lead to a smaller self-acceleration.

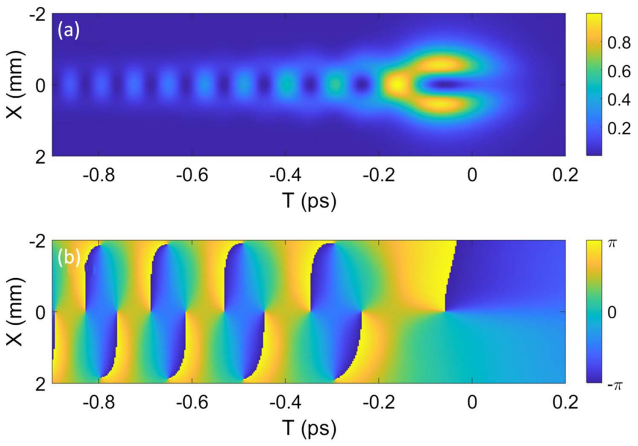

Fig. 1. Simulation of Airy–STOV wave packet. The TOD of $\beta_3 z_0 = 0.00075\ \mathrm{ps}^3$ and the spiral phase of $l = 1$ have been added to the Gaussian pulse with the full width at half-maximum duration of 45 fs. (a) Normalized intensity profile; (b) phase map.

3. Experimental Results

3.1. Generation of Airy–STOVs

The experimental setup to generate the Airy–STOV is very similar to the pulse-shaper setup with a 2D spatial light modulator (SLM) in Ref. [8]. The experimental setup and phase patterns on the SLM are shown in Fig. 2. The surface of the SLM can be understood as the spatial-frequency–frequency domain. To generate the Airy–STOV, a spiral phase and a cubic frequency phase are applied. Since the seed pulse is positively chirped, a quadratic frequency phase is applied to compensate for the residual chirp of the seed pulse. The spatial quadratic phase is also added to compensate for the diffraction effect of the free-space propagation.

To diagnose the Airy–STOV wave packet, the three-dimensional (3D) measurement technique in Ref. [29] is used. For the generated Airy–STOV, a short coherent reference pulse can be overlapped and scanned to retrieve the 3D profile of the Airy–STOV wave packet. The experimental iso-intensity of a typical Airy–STOV shown in Fig. 3(b) is in good agreement with the simulated profile.

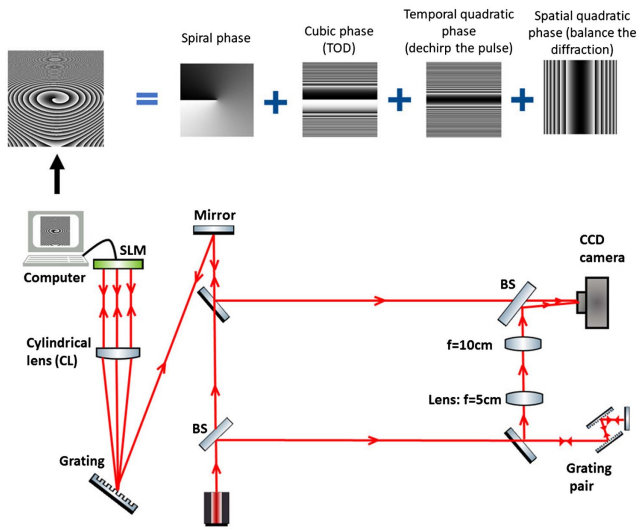

Fig. 2. Experimental setup to generate the Airy–STOV.

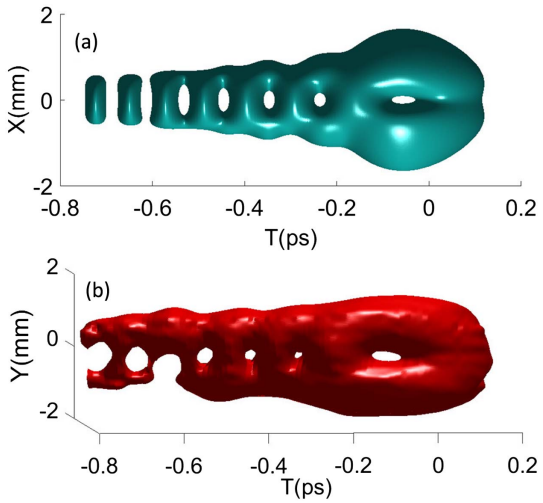

Fig. 3. Generation of Airy–STOV, $\beta_3 z_0 = 0.00075$ ps^3, $l = 1$, $I_{iso} = I_{max}/15$. (a) Simulated iso-intensity plot; (b) experimental iso-intensity plot.

3.2. Properties of Airy–STOVs

3.2.1. Dispersion-free effect

We borrowed the dispersion length (L_D) concept of the Gaussian pulse to estimate the amount of GVD applied in the Airy–STOV propagation. To demonstrate the dispersion-free propagation, the regular STOV without the Airy temporal structure and the Airy–STOV have been compared. The numerical simulations show that regular STOV dramatically broadens in time to lose the integrity of its spatiotemporal phase singularity [Figs. 4(a) and 4(c)] when a significant GVD ($3.7L_D$) is applied. The amount of GVD is expressed in terms of the dispersion length of a Gaussian pulse with the same temporal duration of the STOV at $1/e$ of maximum intensity, which is 57 fs. In contrast, under the same amount of GVD propagation, the numerical simulation shows that the Airy–STOV has much less distortion while maintaining the spatiotemporal phase singularities intact [Figs. 4(b) and 4(d)].

The experimental result [Fig. 4(e)] verifies the dispersion-free propagation showing that the Airy–STOV maintains the main lobe and the phase singularity in $3.7L_D$ propagation. The experimentally measured wave packet matches very well with the simulation results.

3.2.2. Self-acceleration effect

The self-acceleration effect allows us to control the temporal location of the spatiotemporal vortex. According to Eq. (4), the temporal shift is proportional to the square of the propagation distance, which appears as a uniform acceleration motion. We compared the simulation and experimental results again in a strong GVD propagation. The simulated intensity profiles show the temporal shift of zero-intensity holes [Figs. 5(a1)–5(g1)]. Along with zero-intensity holes, the phase singularities are also temporally shifted [Figs. 5(a2)–5(g2)]. The simulation indicates that we can manipulate the temporal location of spatiotemporal singularities. In the experiment, we observed very similar temporal shifts of Airy–STOV in a dispersive propagation [Figs. 5(a3)–5(g3)]. The TOD of 0.0005 ps^3 is applied on the SLM, while the GVD is adjusted in the range of 0.009 ps^2 to −0.009 ps^2.

Figure 6 shows the temporal shift of the phase singularity in the main lobe of the Airy–STOV due to the free acceleration. The simulation and experiment have a similar temporal shift of the phase singularity, which verifies the free-acceleration feature.

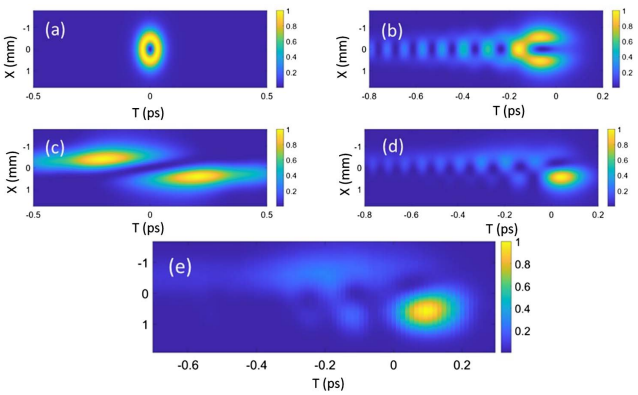

Fig. 4. Comparison between a regular STOV and an Airy–STOV ($\beta_3 z_0 = 0.00075$ ps^3, $l = 1$) under a significant GVD of $\beta_2 z = 0.012$ ps^2 ($3.7L_D$ calculated based on the STOV temporal radius). (a) Simulated regular STOV; (b) simulated Airy–STOV; (c) simulation of the regular STOV under dispersion; (d) simulated dispersion-free propagation of the Airy–STOV; (e) experimental demonstration of dispersion-free propagation of the Airy–STOV.

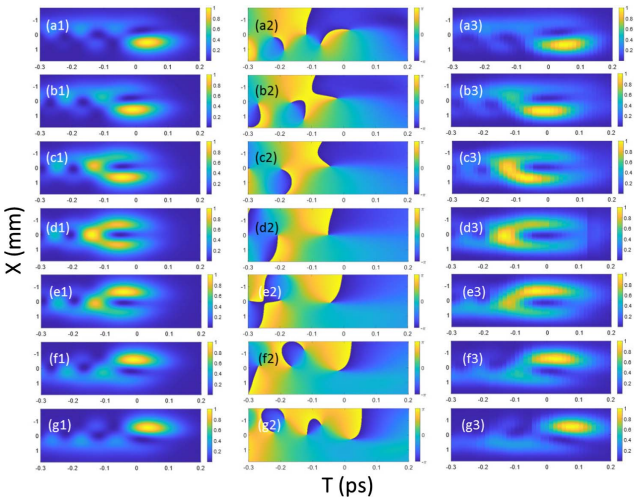

Fig. 5. Simulated and experimental results to demonstrate the self-acceleration effect of the Airy STOV ($\beta_3 z_0 = 0.0005$ ps^3, $l = 1$).(a1)–(g1) Simulated intensity plots; (a2)–(g2) simulated phase plots; (a3)–(g3) experimental intensity plots. (a1)–(a3) $\beta_2 z = 0.009$ ps^2; (b1)–(b3) $\beta_2 z = 0.006$ ps^2; (c1)–(c3) $\beta_2 z = 0.003$ ps^2; (d1)–(d3) $\beta_2 z = 0$ ps^2; (e1)–(e3) $\beta_2 z = -0.003$ ps^2; (f1)–(f3) $\beta_2 z = -0.006$ ps^2; (g1)–(g3) $\beta_2 z = -0.009$ ps^2.

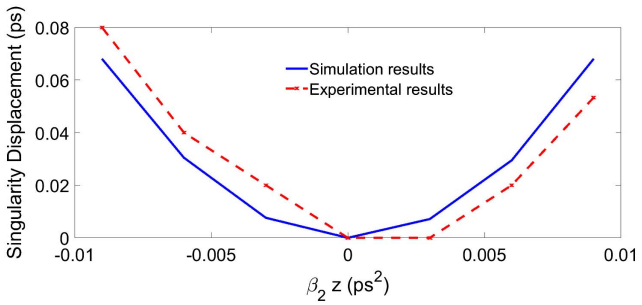

Fig. 6. Simulated (blue solid line) and experimental (red dashed line) phase singularity temporal shift as a function of GVD, $\beta_3 Z_0$ = 0.0005 ps^3.

It is noteworthy that asymmetric intensity distribution occurs around the main lobe phase singularity in the dispersive propagation (Fig. 5). For a normal GVD (GVD > 0), in the main lobe, the energy flows from the upper to the lower part around the singularity and vice versa for the anomalous dispersion. Such an intensity shift is the consequence of the unbalanced dispersion and diffraction effect[8,9]. This result indicates that one can control the spatial intensity distribution with a spectral phase (GVD) revealing the spatiotemporally coupled aspect of the Airy–STOV.

3.2.3. Self-healing effect

Owing to the self-healing feature of the Airy wave pulses, the Airy–STOV also can recover its temporal structure in a dispersive propagation. Figure 7 shows the simulation result and the experimental result of the Airy–STOV self-healing. Figures 7(a) and 7(b) show the initial Airy–STOV with strong intensity around the main lobe singularity. In the Airy pulse, the center frequency is concentrated in the main lobe while the tail contains the red and blue parts of the spectrum. To induce a significant distortion in the main lobe of the Airy–STOV, the center frequency has been filtered out[30]. Figures 7(c) and 7(d) show the simulated and experimental profiles with a strong perturbation in the main lobe after the spectral filtering.

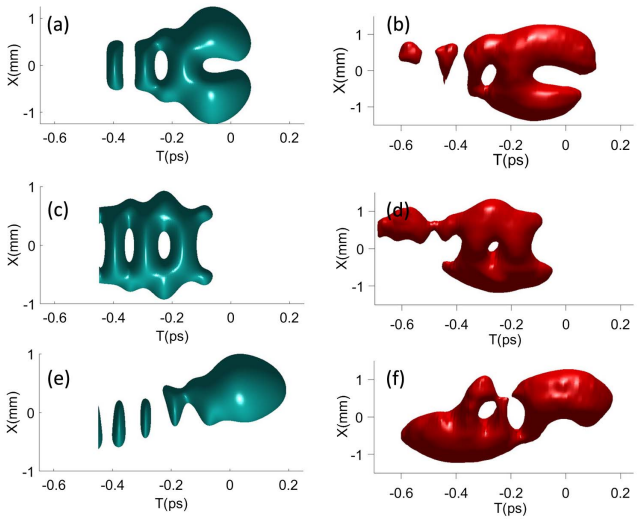

Fig. 7. (a), (c), (e) Simulated and (b), (d), (f) experimental demonstration of the self-healing, $I_{iso} = I_{max}/5$: (a), (b) initial Airy–STOV; (c), (d) disturbed Airy–STOV (center frequency blocked); (e), (f) healed Airy–STOV with GVD of 0.0129 ps^2.

In the experiment, the disturbed wave packet has propagated in a 4-inch (1 inch = 2.54 cm) SF11 glass, which provides the GVD of 0.0129 ps^2. After the propagation in a highly dispersive glass, the main lobe of the Airy–STOV heals to gain the power around the main lobe singularity. The self-healed main lobe has an asymmetry intensity distribution due to the unbalanced dispersion and diffraction. However, it is clear that the Airy–STOV recovers the energy around the main lobe phase singularity due to the self-healing effect [Figs. 7(e) and 7(f)]. Quantitatively, we can calculate the ratio of the OAM of the main lobe to the entire wave packet to analyze the process of the self-healing. The initial transverse OAM of the main lobe to the entire Airy–STOV's OAM is ~30%. After filtering out the center frequency, the main lobe only contains ~8% of the total transverse OAM. After the self-healing in a dispersive medium, the main lobe gains OAM back to ~22% of the total transverse OAM. Interestingly, this observation indicates that the OAM can flow temporally within the wave packet during the dispersive propagation.

4. Conclusion

We demonstrated theoretically and experimentally that phase singularities in the Airy–STOV wave packet have properties of being dispersion-free, self-accelerating, and self-healing, inherited from the Airy pulse propagation. These effects can benefit future applications of STOVs. Due to the dispersion-free feature, it is believed that the Airy–STOVs can maintain the vortex structure even in a lengthy dispersive medium. Owing to the self-healing, Airy–STOVs are likely to be more robust against perturbations. The self-acceleration can be used to control the temporal locations of spatiotemporal singularities. Further, we can extend this concept to a family of wave packets such as Airy–Airy–Airy–STOVs and Airy–Bessel–STOVs, to enhance the maneuverability of the phase singularities.

Acknowledgement

This work was supported by the Pusan National University Research Grant, 2022, and the National Research Foundation of Korea (NRF) funded by the Korea government (MSIT) (No. 2022R1A2C1091890).

References

1. Y. Shen, X. Wang, Z. Xie, C. Min, X. Fu, Q. Liu, M. Gong, and X. Yuan, "Optical vortices 30 years on: OAM manipulation from topological charge to multiple singularities," Light Sci. Appl. **8**, 90 (2019).
2. J. Wang and Y. Liang, "Generation and detection of structured light: a review," Front. Phys. **9**, 263 (2021).
3. A. Forbes, M. de Oliveira, and M. R. Dennis, "Structured light," Nat. Photonics **15**, 253 (2021).

4. J. Wang, "Advances in communications using optical vortices," Photonics Res. **4**, B14 (2016).
5. N. B. Simpson, L. Allen, and M. J. Padgett, "Optical tweezers and optical spanners with Laguerre–Gaussian modes," J. Mod. Opt. **43**, 2485 (1996).
6. S. Fürhapter, A. Jesacher, S. Bernet, and M. Ritsch-Marte, "Spiral phase contrast imaging in microscopy," Opt. Express **13**, 689 (2005).
7. L. Allen, M. W. Beijersbergen, R. J. C. Spreeuw, and J. P. Woerdma, "Orbital angular momentum of light and the transformation of Laguerre-Gaussian laser modes," Phys. Rev. A **45**, 8185 (1992).
8. A. Chong, C. Wan, J. Chen, and Q. Zhan, "Generation of spatiotemporal optical vortices with controllable transverse orbital angular momentum," Nat. Photonics **14**, 350 (2020).
9. S. Hancock, S. Zahedpour, A. Goffin, and H. M. Milchberg, "Free-space propagation of spatiotemporal optical vortices," Optica **6**, 1547 (2019).
10. H. E. Hernandez-Figueroa, M. Zamboni-Rached, and E. Recami, *Localized Waves* (Wiley, 2008).
11. Q. Cao, J. Chen, K. Lu, C. Wan, A. Chong, and Q. Zhan, "Non-spreading Bessel spatiotemporal optical vortices," Sci. Bull. **67**, 133 (2021).
12. M. V. Berry and N. L. Balazs, "Non spreading wave packets," Am. J. Phys. **47**, 264 (1979).
13. G. A. Siviloglou, J. Broky, A. Dogariu, and D. Christodoulides, "Observation of accelerating Airy beams," Phys. Rev. Lett. **99**, 213901 (2007).
14. G. Silviloglou and D. Christodoulides, "Accelerating finite energy Airy beams," Opt. Lett. **32**, 979 (2007).
15. J. Broky, G. A. Siviloglou, A. Dogariu, and D. N. Christodoulides, "Self-healing properties of optical Airy beams," Opt. Express **16**, 12880 (2008).
16. R. Cao, Y. Yang, J. G. Wang, J. Bu, M. W. Wang, and X. C. Yuan, "Microfabricated continuous cubic phase plate induced Airy beams for optical manipulation with high power efficiency," Appl. Phys. Lett. **99**, 261106 (2011).
17. J. Baumgartl, M. Mazilu, and K. Dholakia, "Optically mediated particle clearing using Airy wavepackets," Nat. Photonics **2**, 675 (2008).
18. T. Vettenburg, H. I. C. Dalgarno, J. Nylk, C. Coll-Llado, D. E. K. Ferrier, T. Cizmar, F. J. Gunn-Moore, and K. Dholakia, "Light-sheet microscopy using an Airy beam," Nat. Methods **11**, 541 (2014).
19. Y. Hu, P. Zhang, C. Lou, S. Huang, J. Xu, and Z. Chen, "Optimal control of the ballistic motion of Airy beams," Opt. Lett. **35**, 2260 (2010).
20. Z. Zheng, B. Zhang, H. Chen, J. Ding, and H. Wang, "Optical trapping with focused Airy beams," Appl. Opt. **50**, 43 (2011).
21. K. Cheng, X. Zhong, and A. Xiang, "Propagation dynamics and optical trapping of a radial Airy array beam," Optik **125**, 3966 (2014).
22. M. Chen, S. Huang, X. Liu, Y. Chen, and W. Shao, "Optical trapping and rotating of micro-particles using the circular airy vortex beams," Appl. Phys. B **125**, 184 (2019).
23. Z. Chen and Y. Jiang, "Dual optical trap created by tightly focused circularly polarized ring Airy beam," J. Quant. Spectrosc. Radiat. Transfer **244**, 106851 (2020).
24. X. Peng, Y. Peng, D. Li, L. Zhang, J. Zhuang, F. Zhao, X. Chen, X. Yang, and D. Deng, "Propagation properties of spatiotemporal chirped Airy Gaussian vortex wave packets in a quadratic index medium," Opt. Express **25**, 13527 (2017).
25. Z. Fang, Y. Chen, Y. Ren, L. Gong, R. Lu, A. Zhang, H. Zhao, and P. Wang, "Interplay between topological phase and self-acceleration in a vortex symmetric airy beam," Opt. Express **26**, 7324 (2018).
26. Y. Qian, Y. Shi, W. Jin, F. Hu, and Z. Ren, "Annular arrayed-airy beams carrying vortex arrays," Opt. Express **27**, 18085 (2019).
27. R. A. Suarez, A. A. Neves, and M. R. Gesualdi, "Generation and characterization of an array of airy-vortex beams," Opt. Commun. **458**, 124846 (2020).
28. M. Miyagi and S. Nishida, "Pulse spreading in a single-mode fiber due to 3rd-order dispersion," Appl. Opt. **18**, 678 (1979).
29. H. Li, I. V. Bazarov, B. M. Dunhan, and F. W. Wise, "Three-dimensional laser pulse intensity diagnostic for photoinjectors," Phys. Rev. ST Accel. Beams. **14**, 112802 (2011).
30. A. Chong, W. H. Renninger, D. N. Christodoulides, and F. W. Wise, "Airy–Bessel wave packets as versatile linear light bullets," Nat. Photonics **4**, 103 (2010).